ARTICLES

Microscopic Details of Rotational Diffusion of Perylene in Organic Solvents: Molecular Dynamics Simulation and Experiment vs Debye−Stokes−Einstein Theory

Gouri S. Jas,*,† Erica J. Larson, Carey K. Johnson, and Krzysztof Kuczera*

Departments of Chemistry and Molecular Biosciences, University of Kansas, 2010 Malott Hall, Lawrence, Kansas 66045

Received: April 20, 2000; In Final Form: August 14, 2000

Molecular dynamics simulations and time-resolved linear dichroism measurements have been employed to investigate rotational diffusion of perylene in two organic solvents, cyclohexane, a nonpolar solvent, and 2-propanol, a polar solvent. Both experiments and simulations yield a biexponential rotational anisotropy decay for the long in-plane axis. The calculated time constants were 9 and 44 ps in cyclohexane at 300 K, 13 and 75 ps in 2-propanol at 300 K, and 25 and 126 ps in 2-propanol at 263 K, in excellent agreement with corresponding time-resolved linear dichroism measurements of 14 and 52 ps, 10 and 51 ps, and 22 and 240 ps respectively. Although the viscosity of 2-propanol is more than two times that of cyclohexane at room temperature, the measured rotational reorientation times and the calculated average rotational diffusion coefficients of perylene are similar in the two solvents, demonstrating a breakdown of simple hydrodynamic theory. Analysis of the calculated rotational diffusion coefficients for the individual molecular axes showed that diffusion was highly anisotropic, with the fastest rotation around the out-of-plane axis z. This dominant motion occurred at comparable rates for perylene in cyclohexane and 2-propanol, leading to similar values of average rotational diffusion coefficients in the two solvents. The hindered spinning of perylene in cyclohexane relative to 2-propanol could be rationalized in terms of tighter packing of the former solvent around the solute in the molecular plane.

Introduction

The rotational relaxation of molecules in solution depends on their interactions with the surrounding solvent. As a result, studies of rotational diffusion are a potentially rich source of information on solute−solvent interactions. Investigation of molecular diffusion requires an understanding of the relationship between diffusion and friction.[1−5] Experimentally, diffusion coefficients may be extracted from measurements involving e.g. fluorescence depolarization, time-resolved linear dichroism, light scattering or nuclear magnetic resonance. Diffusion coefficients for rigid particles of various shapes may also be calculated from hydrodynamic theory. Analytical rotational diffusion coefficients have been calculated for spheres[6] and triaxial ellipsoids[7,8] under stick conditions; numerical results were obtained for biaxial[9,10] and triaxial ellipsoids under slip conditions.[11,12] A recent review of current numerical computational results is given by de la Torre and Carrasco.[13] Finally, a microscopic picture of diffusion may be obtained from molecular dynamics (MD) simulations. Numerous simulations of translational and rotational diffusion in molecular systems have been performed on systems ranging from pure liquids[14−17] to proteins.[18] The majority of the previous simulations focus on pure liquid systems, advantageous for their relative simplicity and enhanced sampling. Only a small number of studies, using relatively short simulations, have been performed for solutions.[19−21]

In our previous work, we investigated the rotational diffusion of anthracene as a function of temperature and solvent.[22] The calculated time constants for reorientation were found to be in good agreement with corresponding fluorescence anisotropy decay measurements. The calculated average rotational diffusion coefficients, as well as both calculated and measured rotational reorientation times were close to values predicted for an ellipsoid of shape and size equivalent to an anthracene molecule, and exhibited predictable variation with external conditions − increasing with temperature and decreasing with solvent viscosity. Unexpectedly, the diffusion coefficients around the individual molecular axes of anthracene showed a highly nonuniform variation with both temperature and the type of the solvent. The most striking effect was the change of the character of the dominant motion from tumbling along the long in-plane axis in cyclohexane to spinning around the out-of-plane axis in 2-propanol. This effect has been explained by preferential packing of cyclohexane in the anthracene molecular plane and preferential packing of 2-propanol above and below the plane.[22] Thus, our study showed that the general agreement of the average rotational correlation times with simple theories, often observed for probe molecules[23] may disguise interesting and informative variations in the microscopic details of rotational diffusion around individual axes and their relation to details of solvent structure around the solute.

* To whom correspondence should be addressed. E-mail: kkuczera@ukans.edu and gouri@helix.nih.gov.

† NIDDK, NIH, Bethesda, MD 20892

10.1021/jp001520j CCC: $19.00
Published on Web 10/13/2000

We present here a joint experimental and computational study of the rotational diffusion of perylene in two organic solvents—cyclohexane and 2-propanol. In our approach, the experimental results provide the primary information about the studied phenomenon. The computational models are verified by comparing the calculated and measured values of observable quantities—the relaxation times in time-resolved linear dichroism experiments. Once a reasonable reproduction of the observables has been achieved in the simulations, it is assumed that the computations also realistically describe other aspects of the rotational diffusion, which provide valuable physical insight into the studied phenomena, but which may be difficult to verify experimentally. In our case, we use molecular dynamics simulations to calculate the rates of rotational diffusion around the three molecular axes of perylene in different solvents, and relate some of the observed changes to the three-dimensional distribution of solvent molecules around the reorienting solute. Additionally, the detailed simulation results are used to test the applicability of simple hydrodynamic theories of rotational diffusion in solution. Interestingly, the detailed simulation results show several significant deviations from predictions of simple hydrodynamic theories, showing that specific microscopic effects play an important role in rotational diffusion of perylene molecules in solution.

In the spectroscopic part of the paper, we present time-resolved linear dichroism measurements for perylene in cyclohexane and 2-propanol. The two solvents were chosen to represent two distinct solvent classes, weakly interacting alkanes and self-interacting alcohols, which are known to behave somewhat differently in studies of reorientational motion. Perylene is a good model system for rotational diffusion studies, as two relaxation times may be reliably determined under most experimental conditions. The rotational motion of perylene in organic solvents has previously been studied with transient dichroism[24,25] and two-photon-induced anisotropy decay[26] measurements. A number of studies of perylene rotations in viscous solvents have also been reported.[27−32] Our results are in good general agreement with these experiments, having the additional advantage of improved time resolution.

In the molecular dynamics simulations, we generate trajectories of 2 ns length for perylene motion in both cyclohexane and 2-propanol at 300 K, and of 4 ns length in 2-propanol at 263 K. We use several different calculation methods to obtain both the average diffusion constants and the diffusion rates around each of the molecular axes. In each simulation, we also determine the average three-dimensional solvent distribution around the perylene molecule. Finally, we compare the detailed simulation results with hydrodynamic theory predictions and with the spectroscopic measurements. The simulated decay times for reorientation of the transition dipole axis are in excellent agreement with experimental data. Although the viscosity of 2-propanol is more than two times that of cyclohexane at room temperature, the measured rotational reorientation times and the calculated average rotational diffusion coefficients of perylene are similar in the two solvents, demonstrating a breakdown of simple hydrodynamic theory. The molecular dynamics simulations show that diffusion is highly anisotropic, with the fastest rotation around the out-of-plane axis. This dominant motion occurs at comparable rates for perylene in cyclohexane and 2-propanol, leading to similar values of average rotational diffusion coefficients in the two solvents. The rates of perylene spinning in cyclohexane relative to 2-propanol can be rationalized in terms of tighter packing of cyclohexane in the solute molecular plane. Our study is aimed at improving the basic understanding of molecular diffusion of perylene and related probe molecules. Our results demonstrate the power and usefulness of joint experimental−computational studies, which provide new experimental data, microscopic insight and theoretical analysis of the studied phenomena.

Methods

Time-resolved Linear Dichroism Measurements. The anisotropy decays were obtained with a femtosecond laser system. Pulses from a Kerr lens mode-locked Ti:sapphire oscillator were seeded into a Clark MXR CPA-1 regenerative amplifier. The resulting pulses were centered around 800 nm and had widths of about 150 fs at a 1 kHZ repetition rate. The pulses were divided into pump and probe with a 50/50 beam-splitter, and the probe pulse was delayed with respect to the pump with a computer controlled delay line. The 400 nm excitation source was obtained by frequency doubling the 800 nm pump pulses with a 0.5 mm BBO (β-barium borate) crystal. The pump power at 400 nm was 10−20 mW. The pump beam was chopped at 500 Hz. The pump and probe were either overlapped collinearly or at a small angle. The 800 nm probe pulses were collimated with a telescope and directed into a piece of quartz to generate a continuum, and the desired probe wavelength was selected with an appropriate interference filter. The parallel and perpendicular components of the probe absorption were collected simultaneously. Glan laser polarizers were used to plane polarize the pump and probe beam 45° with respect to each other. The analyzer was a glan laser polarizer with two escape windows, crossed with the pump polarizer. With this arrangement, the component of the probe beam transmitted through the analyzer polarizer was collected and saved as the perpendicular component, while the component that was reflected from the polarizer was collected and saved as the parallel component. A reference beam equal in intensity to the parallel and perpendicular components of the probe was obtained by splitting off a fraction of the probe beam and directing it onto a reference photodiode. The signals from the parallel, perpendicular, and reference photodiodes were processed by Stanford Research Systems gated integrator modules. The integrated values of parallel minus reference, $S_{\parallel} - S_0$, and of perpendicular minus reference, $S_{\perp} - S_0$, were processed by lock-in amplifiers (Stanford Research Systems).

Care was taken to ensure that the parallel and perpendicular intensities of the probe beam were equal in the absence of pump pulses to permit accurate measurement of anisotropies. The relative drifts between the parallel and perpendicular signals, $S_{\parallel}$ and $S_{\perp}$, during the course of the experiment were corrected by use of a shutter in the pump path as follows. Prior to the collection of every tenth point, the shutter blocked the pump beam and the parallel and perpendicular polarization components of the probe, $S_{\parallel}$ (no pump) and $S_{\perp}$ (no pump), were collected. These values were used to adjust the offsets for the next 10 data values. An additional baseline correction was calculated after every tenth shot to correct for scattered light from the pump pulses that was detected because the repetition rate of the chopped pump beam corresponded to the lock-in reference frequency. To correct for the resulting small contribution to the detected signals, the offsets of the gated integrators were set to zero when the probe was blocked and the pump was allowed through. The offset was corrected after every tenth shot via a shutter that blocked the probe beam and allowed a reading of the contribution of the pump beam to the parallel and perpendicular signals to be taken. This offset was then subtracted from the subsequent 10 data values. The transient absorption with

parallel and perpendicular polarization was then calculated in the small signal limit for each shot as

$$\Delta A_{\parallel} = \left(\frac{S_0 - S_{\parallel}}{S_0}\right) - \left(\frac{S_0 - S_{\parallel}}{S_0}\right)_{\text{probe only}} - \left(\frac{S_0 - S_{\parallel}}{S_0}\right)_{\text{pump only}} \quad (1)$$

(and similarly for $\Delta A_{\perp}$). With these precautions, the parallel and perpendicular transient absorption values were reproducibly zero for negative delay times, and the anisotropies decayed to zero at long delay times. The anisotropy at each time delay was obtained from the transient absorption with parallel and perpendicular polarization as

$$r = \frac{\Delta A_{\parallel} - \Delta A_{\perp}}{\Delta A_{\parallel} + 2\Delta A_{\perp}} \quad (2)$$

Thirty laser shots were averaged at each time delay, and 50−100 data points were collected per scan. A total of 25−100 scans were averaged for each experiment. The anisotropy decays were fit to two-exponential functions by nonlinear regression with the Origin software package (Microcal Software, Inc.) using the Levenberg−Marquardt (LM) algorithm.

Zone-refined (99%) perylene was purchased from Aldrich and used as received. Spectral grade solvents 2-propanol (99.9%) and cyclohexane (99%) were purchased from Aldrich and showed no evidence of significant fluorescence under our experimental conditions. These solvents were bubbled with nitrogen gas for 40 min prior to use. The concentrations of perylene solutions were typically $\approx 2 \times 10^{-4}$ M. The fluorescence spectra of the samples showed no sign of perylene aggregation. The sample was flowed through the sample cell to ensure that each laser shot interrogated a fresh volume of solution.

Force Field Parametrization. The CHARMM program (Version 24) was used in the simulations[33] with the version 22 all-hydrogen topology and parameters[34] in which all atoms are treated explicitly. For perylene, all carbons were assigned to the existing CHARMM aromatic carbon type CA, and all hydrogens were assigned to the existing type HP.[34] This assignment defined all force field parameters for internal strain and van der Waals potential energy terms. The atomic charges were obtained from the Mulliken population analysis of the HF/6-31G* optimized D_{2h} structure of perylene[35,36] scaled down by 0.9 to correct for systematic error.[37] With these parameters, the CHARMM optimized geometry of perylene is found to be in good agreement with the crystal structure, with bond length deviations below 0.02 Å and bond angle deviations below 2°. The optimized structure, atomic charges, and molecular axis labels are described in Figure 1.

For cyclohexane the existing CHARMM aliphatic carbons (CT2) and hydrogens (HA) were used with the standard aliphatic charges −0.18 of on methylene carbons and 0.09 on hydrogens (all charges are in atomic units). For 2-propanol the CHARMM topology, parameters and atomic charges from the threonine side chain were used; with atom types CT1 for the CH carbon, CT3 for the methyl group carbons, OH1 for the hydroxyl oxygen, HA for the aliphatic hydrogens and H for the hydroxyl hydrogen.[33] The atomic charges were 0.14 on CT1, −0.66 on OH1, 0.43 on H, −0.27 on CT3, and 0.09 on HA.[33] The properties of pure liquid cyclohexane and 2-propanol modeled by these parameters are in good agreement with with experimental data.[38]

Molecular Dynamics Simulation Protocol. The initial structure of perylene was taken from the CHARMM optimized

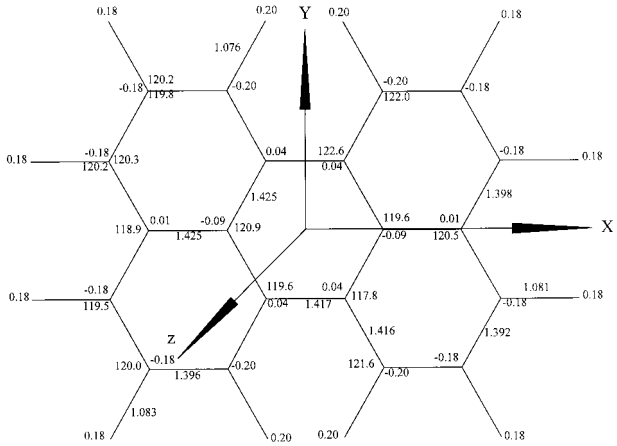

Figure 1. Perylene geometry and molecular axis system. Bond lengths in Å, angles in degrees, charges in Au.

geometry. Truncated cubic cells with 166 cyclohexanes and 235 2-propanols were equilibrated at 300 K and constant volume, with densities corresponding to 1 atm pressure (densities used: 0.7762 g/cm^3 for cyclohexane 0.7832 g/cm^3 for 2-propanol[39]). After replacing two solvent molecules with perylene and correcting for the difference in molecular volume between solute and solvent at 300 K, the cyclohexane solution system thus contained one perylene and 164 cyclohexane molecules in a truncated cubic cell based on a cube of side 39.1003 Å, whereas the 2-propanol system contained one perylene and 232 2-propanol molecules in a cell based on a cube of side 39.1249 Å. The CHARMM van der Waals volume of perylene (296 Å ^{3}) was used in the correction. An analogous procedure was performed for perylene in 2-propanol at 263 K. Because our simulations were performed under constant pressure conditions, the box dimensions automatically adjusted by 0.1−0.2 Å during the equilibration phase to reflect the desired average pressure of 1 atm. In all molecular dynamics (MD) simulations, SHAKE constraints[40] were introduced on the bonds involving hydrogen atoms, allowing use of a 2 fs time step.[41] In energy calculation, a 12.0 Å atom based nonbonded cutoff distance was used, with a switching function between 10.0 and 12.0 Å for van der Waals terms and a shift function at 12.0 Å for electrostatics in order to eliminate discontinuities due to the cutoff. Each simulation system was prepared by energy minimization, 10 ps of heating by random velocity assignments at stepwise increasing temperatures and 10 ps equilibration at the target temperature, 263 and 300 K in 2-propanol, and 300 K in cyclohexane. This was followed trajectory generation: 4 ns for the 2-propanol system at 263 K, and 2 ns in the 300 K simulations in cyclohexane and 2-propanol. The Verlet algorithm was used for integration of equations of motion in all simulations.[42] Periodic boundary conditions were applied and the simulation conditions corresponded to the NPT ensemble. The average pressure was held at 1 atm using the Langevin piston method, with piston mass of 100.0 amu and collision frequency of 10 ps^{-1}.[43] The average temperature was held at the desired target value, 263 or 300 K, using the Hoover algorithm with a coupling parameter of 250 kcalA ps^2.[44] The average temperature fluctuations were 4 K in all three trajectories. Coordinates and velocities of all atoms were saved every 0.05 ps for analysis.

Rotational Diffusion Analysis. Rotational diffusion coefficients of perylene, D_r, are calculated using four methods, based on reorientation of the molecule as a whole, reorientation of the individual molecular axes and angular velocity autocorrelation functions (AVACF) in the laboratory (LAB) and molecular (MOL) frames. In the first method, the expression[45] $D_r =$

TABLE 1: Average Rotational Diffusion Coefficients of Perylene in Cyclohexane (300 K) and in 2-propanol (263 and 300 K)[a]

		average: D_r				Theory				
solvent	T (K)	CM Rot.[b]	LAB AVACF[c]	MOL AVACF[e]	C_1[d]	Sph	A	B	C	D
2-propanol	263	0.0025 ± 0.0011	0.0035 ± 0.0012	0.0042 ± 0.0012	0.0023 ± 0.0007	0.0004	0.0014	0.0020	0.0028	0.0032
	300	0.0077 ± 0.0012	0.0075 ± 0.0032	0.0112 ± 0.0022	0.0073 ± 0.0008	0.0012	0.0044	0.0063	0.0085	0.0103
Cyclohexane	300	0.0074 ± 0.0043	0.0107 ± 0.0023	0.0127 ± 0.0033	0.0082 ± 0.0007	0.0027	0.0105	0.0151	0.0203	0.0245

[a] Units: rad^2/ps. [b] CM Rot: Center of Mass Rotation [c] LAB AVACF: angular velocity autocorrelation function in the laboratory fixed frame. [d] C_1 autocorrelation functions of molecular axes. [e] MOL AVACF: angular velocity autocorrelation function in the molecule fixed frame; Sph: sphere with stick boundary condition. A. Asymmetric ellipsoid (1:0.7:0.3) with slip boundary condition; B. Asymmetric ellipsoid (1:0.7:0.4) with slip boundary condition; C. Asymmetric ellipsoid (1:0.8:0.3) with slip boundary condition; D. Asymmetric ellipsoid (1:0.8:0.4) with slip boundary condition.

$\langle \Delta\theta^2(t)\rangle/6t$ was used, where $\Delta\theta(t)$ is the angle of rotation of the molecule-fixed frame during time t and $\langle\cdots\rangle$ is an average over initial positions. The reorientation angle between two perylene structures is calculated by overlaying them in the root-mean-square sense using the CHARMM program.[33] We calculated D_r from the slope of $\langle \Delta\theta^2(t)\rangle$ in its region of linear behavior, 5−40 ps.

In the LAB AVACF method, the angular velocity time series $\vec{\omega}(t)$ of rotation around the perylene CM is calculated from the trajectory as $\vec{\omega}(t) = \boldsymbol{I}(t)^{-1}\cdot\vec{L}(t)$, where $\boldsymbol{I}(t)^{-1}$ is the inverse of the instantaneous moment of inertia tensor, and $\vec{L}(t)$ is the angular momentum relative to the molecular CM. The diffusion coefficient is then calculated from the integral[46,47]

$$D_r = \frac{1}{3}\int_0^{\tau_r} dt\langle\vec{\omega}(0)\cdot\vec{\omega}(t)\rangle \qquad (3)$$

The calculated D_r values exhibit some dependence on the upper limit τ_r of the integral. To eliminate this dependence, the average value of the integral for τ_r between 5 and 15 ps was used. This choice was based on analysis of the data: the calculated AVACF tended to fluctuate around zero for times above 3 ps; the AVACF evaluated separately from the two halves of the simulation tended to become uncorrelated for time longer than 5 ps; finally, for times longer than 5 ps, the calculated integrals tended to fluctuate around stable values. In the MOL AVACF approach, the perylene angular velocity time series was transformed to the molecular frame (MOL), defined by the principal axes of the instantaneous moment of inertia tensor $\boldsymbol{I}(t)$. This allowed the calculation of rotational diffusion coefficients along individual molecular axes[46,47]

$$D_i = \int_0^{\tau_r} dt\langle\omega_i(0)\cdot\omega_i(t)\rangle,\ i = x, y, z \qquad (4)$$

as well as their average $D_r = (D_x + D_y + D_z)/3$. In all the calculation methods above, the statistical errors of D_r are estimated as half the difference between values obtained by using data from the two halves of the simulation separately.

Rotational diffusion coefficients of perylene are also derived from correlation functions $C_{1,i}(t)$ for the reorientation of molecular axes, $i = x, y, z$. For a unit vector $\vec{n} = (n_x, n_y, n_z)$ rotating with the molecule we define: $C_1(t) = \langle\vec{n}(0)\cdot\vec{n}(t)\rangle$. For a molecule of high symmetry, such as perylene, we expect that the principal axes of the moment of inertia and diffusion tensors will coincide. We thus evaluate the time series of the principal axis directions of the perylene molecule $n_i(t)$, i=x, y, z, and evaluate their correlation functions $C_{1,i}(t)$. In this case, rotational diffusion theory predicts that[48]

$$C_{1,i}(t) = e^{-(3D_r - D_i)t},\ i = x, y, z \qquad (5)$$

The calculated $C_{1,i}(t)$ functions were fitted to single-exponential decays and the rotational diffusion coefficients around the individual molecular axes D_i derived from the exponents. The statistical errors of the exponents derived from the $C_{1,i}(t)$, correlation functions were estimated to be $\sqrt{2\tau_i/T_{tot}}$, where $1/\tau_i = 3D_r - D_i$, and T_{tot} is the total simulation time.[45] The errors of D_x, D_y, and D_z were estimated by error propagation.

Calculation of Rotational Relaxation Times. Experimental methods for studying rotational diffusion measure quantities related to the correlation function $C_2(t) = \langle 3(\vec{n}(0)\cdot\vec{n}(t))^2 - 1\rangle/2$ where $\vec{n} = (n_x, n_y, n_z)$ is a vector rotating with the molecule. For example, the fluorescence anisotropy decay for parallel absorption and emission transition dipoles is given by[48,49] $r(t) = (I_{||}(t) - I_{\perp}(t))/(I_{||}(t) + 2I_{\perp}(t)) = (2/5)C_2(t)$, where $I_{||}$ and $I_{\perp}$ are the intensities of emitted light with polarization parallel and perpendicular to that of the exciting pulse and $C_2(t)$ is the correlation function of the emission dipole axis. Similar expressions hold for methods based on linear dichroism and transient absorption.[49]

Assuming that perylene reorientations have diffusional character and the molecular axes are also principal axes of the diffusion tensor, for transition dipoles oriented along the x, y, or z, we expect a biexponential decay for C_2[48,49]

$$C_{2,i}(t) = a_i e^{-(6D_r + 2\Delta)t} + b_i e^{-(6D_r - 2\Delta)t},\ i = x, y, z \qquad (6)$$

where D_r is the average rotational diffusion coefficient,

$$\Delta = (\sqrt{D_x^2 + D_y^2 + D_z^2 - D_xD_y - D_xD_z - D_yD_z}) \qquad (7)$$

is a measure of the anisotropy, and the factors a_i, b_i are functions of D_x, D_y and D_z. The inverses of exponents in the above equation are often called the rotational relaxation times: $\tau_1 = 1/(6D_r + 2\Delta)$ and $\tau_2 = 1/(6D_r - 2\Delta)$. Interestingly, the two exponents are the same for all three axes, only their contributions to C_2 differ. If one of the coefficients a_i or b_i is small, a single-exponential decay of C_2 may be observed, even if both times τ_1 and τ_2 fall into the experimentally accessible time range.[49]

We have calculated the correlation functions $C_{2,i}(t)$, $i = x, y, z$ for the principal axes of the instantaneous moment of inertia tensor $I(t)$ of perylene to directly compare with the experimental results. These $C_{2,i}(t)$ functions are then fitted to a two-exponential function in order to obtain τ_1 and τ_2. In Table 3 we present the time constants for τ_1 and τ_2 of the long axis (x) as the transition dipole moment of perylene is directed along long-axis.

We also used the individual diffusion coefficients D_x, D_y, and D_z determined from fitting the $C_1(t)$ correlation functions and the MOL AVACF in conjunction with the formulas[47] to obtain separate computational estimates of τ_1, τ_2 and the weights a_i,

TABLE 2: Rotational Diffusion Coefficients around Individual Molecular Axes of Perylene in Cyclohexane (300 K) and in 2-propanol (263 and 300 K) Units: Rad²/ps

T (K)		MOLAVACF[a]	C_1[b]	A	B	C	D
			2-propanol				
263							
	D_x	0.0049 ± 0.0035	0.0019 ± 0.0012	0.0009	0.0021	0.0006	0.0013
	D_y	0.0021 ± 0.0028	0.0008 ± 0.0011	0.0004	0.0006	0.0008	0.0007
	D_z	0.0055 ± 0.0047	0.0041 ± 0.0013	0.0029	0.0032	0.0069	0.0077
300							
	D_x	0.0086 ± 0.0018	0.0036 ± 0.0014	0.0028	0.0067	0.0020	0.0041
	D_y	0.0058 ± 0.0012	0.0015 ± 0.0012	0.0012	0.0020	0.0012	0.0021
	D_z	0.0193 ± 0.0019	0.0167 ± 0.0013	0.0092	0.0103	0.0224	0.0248
			cyclohexane				
300							
	D_x	0.0129 ± 0.0018	0.0062 ± 0.0012	0.0067	0.0158	0.0048	0.0097
	D_y	0.0053 ± 0.0013	0.0034 ± 0.0011	0.0028	0.0049	0.0029	0.0050
	D_z	0.0198 ± 0.0019	0.0150 ± 0.0013	0.0219	0.0246	0.0532	0.0588

[a] MOLAVACF: angular velocity autocorrelation function in the molecular fixed frame. [b] C_1 autocorrelation function of molecular axis. A. Slip hydrodynamics, axis ratio 1:0.7:0.3; B. Slip hydrodynamics, axis ratio 1:0.7:0.4; C. Slip hydrodynamics, axis ratio 1:0.8:0.3; D. Slip hydrodynamics, axis ratio 1:0.8:0.4.

TABLE 3: Rotational Relaxation Times of Perylene in Cyclohexane and in 2-Propanol from Simulations and Hydrodynamic Models[a]

	2-propanol						cyclohexane		
	263 K			300 K			300 K		
	τ_1	τ_2	a^b	τ_1	τ_2	a^b	τ_1	τ_2	a^b
C_1	51 ± 30	128 ± 80	0.6,0.9,0.0	14 ± 3	66 ± 30	0.7,0.8,0.0	14 ± 3	35 ± 20	0.6,0.8,0.0
$C_{2,x}$	25 ± 4	126 ± 30		13 ± 3	75 ± 21		9 ± 4	44 ± 9	
A	77	145		24	85		10	36	
B	61	137		19	42		8	18	
C	34	238		11	104		4	43	
D	30	167		9	54		4	23	

[a] Units: ps. [b] calculated weights of τ_1 exponent in C_{2x}, C_{2y}, C_{2z}. $C_2(t) = a \exp(-t/\tau_1) + (1 - a) \exp(-t/\tau_2)$. A = Slip hydrodynamics, axis ratio 1:0.7:0.3; B = Slip hydrodynamics, axis ratio 1:0.7:0.4; C = Slip hydrodynamics, axis ratio 1:0.8:0.3; D = Slip hydrodynamics, axis ratio 1:0.8:0.4.

b_i. Finally, to correlate our results with theoretical models of rotational diffusion, we used the predicted values of D_x, D_y, and D_z for a triaxial ellipsoid under slip conditions[11,12] to obtain relaxation times based on hydrodynamic theory.

Solvent Distribution Analysis. The three-dimensional (3D) distribution of the solvent molecules around perylene was analyzed by repeating the following procedure for each trajectory frame: (a) generating positions of all solvent molecules within 19 Å of the perylene solute, including image molecules if needed, (b) orienting coordinates of all the atoms to the principal axis system of the instantaneous moment of inertia of the solute, and (c) counting and accumulating the distribution of solvent atoms (or alternatively: solvent centers-of-mass) on a 3D cubic grid of 1 Å side within a range of ±19 Å from the solute center. Comparing the number of counts to that expected for a pure solvent with known molecular volume provides a graphical representation of regions of enhanced or diminished solvent density.

Estimates of Perylene Size and Shape. We used two methods to estimate perylene size and shape, based on the van der Waals volume and excluded volume. Using CHARMM van der Waals radii,[33] we obtain molecular dimensions of 12.0, 9.5, and 4.0 Å along the three principal axes. These results indicate that the molecule may be described as a triaxial ellipsoid with axis ratios of 1.0:0.79:0.33. The volume enclosed within the van der Waals radii of perylene is 296 Å^3, as calculated by CHARMM.[33] A separate estimate of size and shape was made by calculating the average volume free of solvent atoms in the simulations. This was done by a method analogous to the 3D solvent distribution calculation with the difference being in the use of a finer cubic grid of 0.2 Å over a smaller range of coordinates and counting all solvent atoms, including hydrogens. The excluded volume was calculated by analyzing the unoccupied bins around the origin. The excluded volumes were quite similar in all three trajectories, falling in the 364−387 Å^3 range. In both of the 2-propanol simulations, the molecular dimensions were 13.1, 10.9, and 4.9 Å along the three principal axes, corresponding to an axis ratio of 1.00:0.83:0.37. In the 300 K cyclohexane trajectory, the dimensions were 12.9, 10.4, and 4.9 Å, corresponding to an 1.00:0.81:0.38 axis ratio.

Due to the irregular shapes of the cavities occupied by the solute and the relatively low average number of counts per bin on a 0.2 Å grid, precise results are difficult to obtain. However, several trends may be seen in the data. First, the ellipsoid models of molecular shape are qualitatively similar in excluded volume and van der Waals calculations, with the former having 10−20% larger dimensions, and ca. 30% higher volumes. This is in agreement with experimental findings that partial molar volumes of nonpolar solutes are generally significantly higher than their van der Waals volumes.[50] Second, the solvent-free cavities occupied by perylene in cyclohexane and 2-propanol are quite similar. The only significant difference is the 0.5 Å larger length of the 2-propanol cavity along the in-plane *y* axis.

Results and Discussion

Simulations: Average Diffusion Coefficients. The calculated rotational diffusion coefficients of perylene in solution are given in Tables 1 and 2. Four different methods of calculating the average diffusion coefficient D_r were used (see Methods). Within each simulation all four methods yielded results that

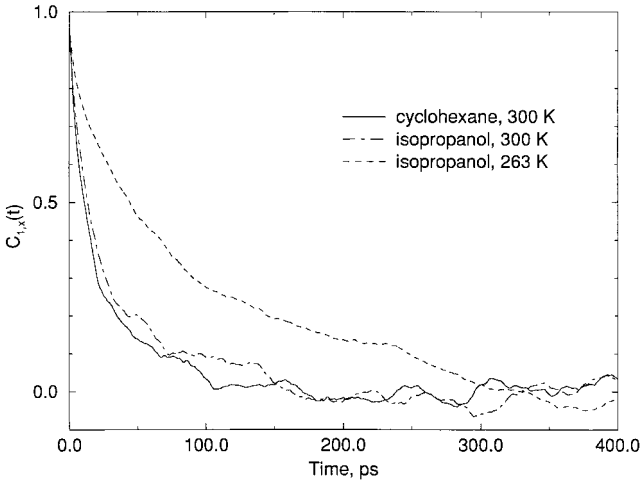

Figure 2. C_1 correlation functions for reorientation of the molecular *X* axis of perylene in cyclohexane (at 300 K) and in 2-propanol (at 263 and 300 K).

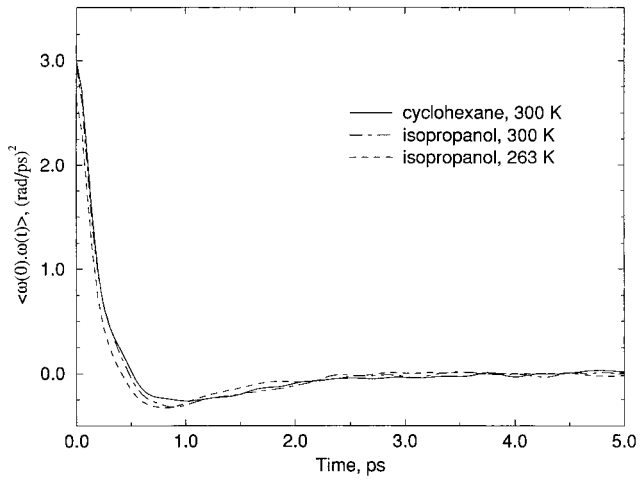

Figure 3. Components of the center-of-mass angular velocity-autocorrelation functions of perylene in cyclohexane (at 300 K) in the molecule fixed axis system.

agreed within their statistical errors. It appears that the LAB AVACF approach yields results that are systematically higher than all the other methods. The mean values of D_r from the three calculation methods were 0.0034, and 0.0088 ps^{-1} in 2-propanol at 263 and 300 K, respectively, and 0.0103 ps^{-1} in cyclohexane at 300 K. Examples of the calculated C_1 correlation functions for axis reorientation and of perylene AVACFs are presented in Figures 2 and 3.

The simplest model of rotational diffusion is that of a sphere of volume *V* moving through a medium of viscosity η with stick boundary conditions; the diffusion coefficient is then given by the Debye−Stokes−Einstein (DSE) formula[1]

$$D_r = \frac{kT}{6\eta V}$$

where *k* is the Boltzmann constant and *T* is the temperature. This model yields the basic hydrodynamic theory predictions that rotational diffusion rates will be inversely proportional to the solvent viscosity, and that they will rise with increasing temperature (both because of the factor *kT* in the numerator and because η is a decreasing function of *T*). Setting $V = 296$ Å^3, the volume enclosed within the van der Waals surface of perylene, and the viscosity to 5.72, 2.02, and 0.85 cP[51], corresponding to pure 2-propanol at 263, and 300 K and pure cyclohexane at 300 K, respectively, we obtain the respective D_r values of 0.0004, 0.0012, and 0.0027 ps^{-1}.

One aspect of our simulation results, the approximately 3-fold increase in D_r of perylene in 2-propanol between 263 and 300 K, is in agreement with DSE predictions. On the other hand, the calculated D_r values of perylene in cyclohexane and 2-propanol at 300 K are in qualitative disagreement with DSE theory. At 300 K, 2-propanol has a viscosity that is about 2.4 times larger than that of cyclohexane. However, the rotational diffusion coefficients of perylene in these two solvents at 300 K are essentially identical within the statistical errors. This indicates a breakdown of simple hydrodynamic predictions based on DSE theory.

Additionally, the calculated diffusion coefficients are about 3−7 times higher than expected from the DSE equation. Similar effects have been found in experimental[52,53,23] and computational studies.[22] These deviations may be explained by two main factors, diffusion anisotropy and deviation of boundary conditions from stick type. Under stick conditions, the effects of anisotropy are predicted to be small. Using Perrin's formulas,[7,8] we obtain a shape factor (equal to the ratio of the rotational friction coefficient to that of a sphere of equal volume) of $F = 1.1$ for an oblate symmetric ellipsoid with axis ratio 0.6, and $F = 1.4$ for an asymmetric ellipsoid with ratio of axes of 1.0:0.83:0.37. Applying these correction factors would decrease the hydrodynamic diffusion coefficients by 10−40%, moving them further away from the calculated results.

A number of simulations and experimental studies suggest that slip boundary conditions may be appropriate for many organic molecules in solution.[20,23,54,55,56] Faster diffusion rates are expected under slip conditions;[54,55] e.g., a symmetric ellipsoid should undergo free rotation around its symmetry axis because such motion displaces no solvent. Using the results of Youngren and Acrivos,[11] as corrected by Hochstrasser and Sension,[12] we obtain diffusion coefficients in better agreement with the calculated results. Using the same solvent viscosities as described above and coefficients from Table 1 of [12] for an ellipsoid with volume $V = 296$ Å^3 and axis ratios 1.0:0.8:0.3 we obtain diffusion coefficients D_r of 0.0028, and 0.0085 ps^{-1} for perylene in 2-propanol at 263 and 300 K, and 0.0203 ps^{-1} in cyclohexane at 300 K. These values are in quite good agreement with our simulation results in 2-propanol. However, the theoretical diffusion coefficient in cyclohexane is almost twice as large as our simulated value. We can improve the agreement of the cyclohexane values by using a slightly modified shape of perylene. For axis ratios of 1.0:0.7:0.3 the hydrodynamic rotational diffusion coefficient in cyclohexane comes out to be 0.0105 ps^{-1}, quite close to our calculated value, but now the coefficients in 2-propanol are underestimated by the theory (see Table 1).

Simulations: Anisotropy. The rotational diffusion coefficients D_x, D_y, D_z of perylene around its three molecular axes are presented in Table 2. The molecular axes of perylene are shown in Figure 1. Calculations were carried out by fitting the first-order correlation functions $C_{1,i}(t)$, $i = x, y, z$ describing the reorientation of the axes (see Methods).

The rotational diffusion of perylene found in the simulations is highly anisotropic, with ratios of greatest to smallest diffusion coefficients ranging from 11:1 to 5:1 (Table 2). Similar ratios are found in the hydrodynamic models A−D in Table 2. As may be expected from hydrodynamic theory for an oblate-like rotor, in all three simulations rotation around the out-of-plane (*z*) axis is the fastest, whereas rotation around the short in-plane axis (*y*) is the slowest. What is unexpected is that the diffusion

coefficients undergo nonuniform changes with temperature and solvent type. For perylene in 2-propanol the variation of D_x, D_y, D_z between 300 and 263 K deviates only mildly from hydrodynamic predictions. The ratio of the factor T/η at these two temperatures is 3.2, whereas D_z decreases by about a factor of 4, and both D_x and D_y by about a factor two. The largest deviations from hydrodynamic predictions appear upon comparing the diffusion coefficients of perylene in 2-propanol and cyclohexane at 300 K. The viscosity of 2-propanol is about 2.2 greater than that of cyclohexane at this temperature. The coefficients D_x and D_y approximately follow this trend, being about two times larger in cyclohexane than in 2-propanol (Table 2). However, the reorientation rates around the z axis are approximately the same for perylene in these two solvents. Because D_z is larger than D_y or D_x, the overall result is only a small change in the average rotational diffusion coefficient D_r between 2-propanol and cyclohexane.

In our previous studies of anthracene in the same two solvents[22] the simulation results for the rotational correlation time τ_1 were also in good agreement with experimental measurements (a single relaxation time is observed in most experiments). Calculated average rotational diffusion coefficients of anthracene followed DSE predictions for a triaxial ellipsoid under slip conditions. However, nonuniform changes with temperature and solvent were found for reorientation rates around individual molecular axes. The most striking effect was the change of the fastest rotational motion of anthracene from tumbling around the long in-plane axis in cyclohexane to spinning around the molecular plane normal in 2-propanol. The selective slowing down of the spinning motion in cyclohexane relative to 2-propanol appears to be the common factor in rotational diffusion of both anthracene and perylene. For both solutes these effects may be explained in terms of local solvent structure, although the details of the mechanism differ, as explained below.

Simulations: Solvent Structure. Due to the large size and relatively complex structure of the solute, we focus on the 3D solvent distributions calculated in the solute-fixed frame (see Methods for details). These distributions provide a powerful description of solvation and reveal several interesting features; they are presented in Figures 4−8.

The results for both cyclohexane and 2-propanol show the presence of a well-defined first solvation shell, which shows up as a band of high solvent density directly surrounding the solute (Figures 4−8). The solvation shells do not appear to have any significant resolvable structure. This would indicate that there is a general clustering of solvent around the solute, but there are few solvent molecules that reside at well-defined locations and are dragged along with the reorienting solute. This is the expected result under slip conditions. The shapes and relative densities of the first solvation shells appear to be quite similar in the two solvents and do not vary noticeably between the 263 and 300 K 2-propanol simulations. More precise measurements of the solvent-excluded cavity occupied by perylene were determined by sampling positions of all solvent atoms on a finer grid, as described in the **Estimates of Perylene Size and Shape** section above. There, the solvent-excluded cavities in cyclohexane and 2-propanol had essentially the same size along the x and z directions. However, the cavity in cyclohexane was smaller than that in 2-propanol by about 0.5 Å in the y direction. Such a difference in microscopic solvent structure would lead to hindered spinning around the z axis in cyclohexane compared to hydrodynamic predictions. This is just the effect that is seen in the simulations.

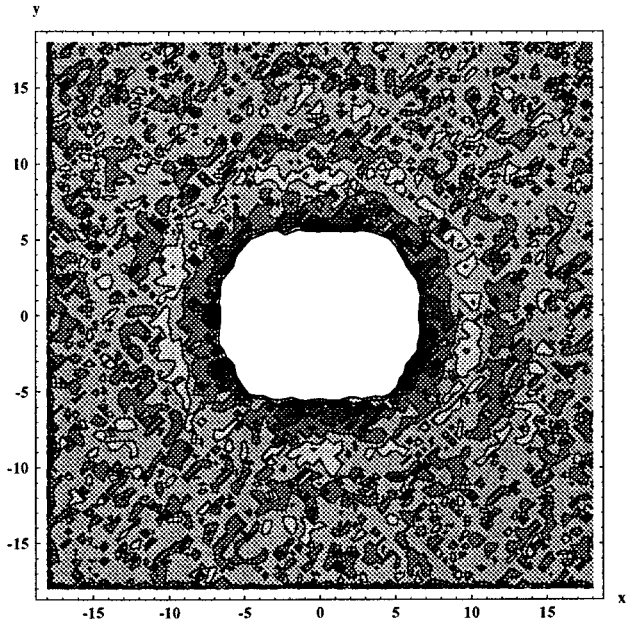

Figure 4. Distribution of cyclohexane carbons around perylene: slice in XY plane, 300 K.

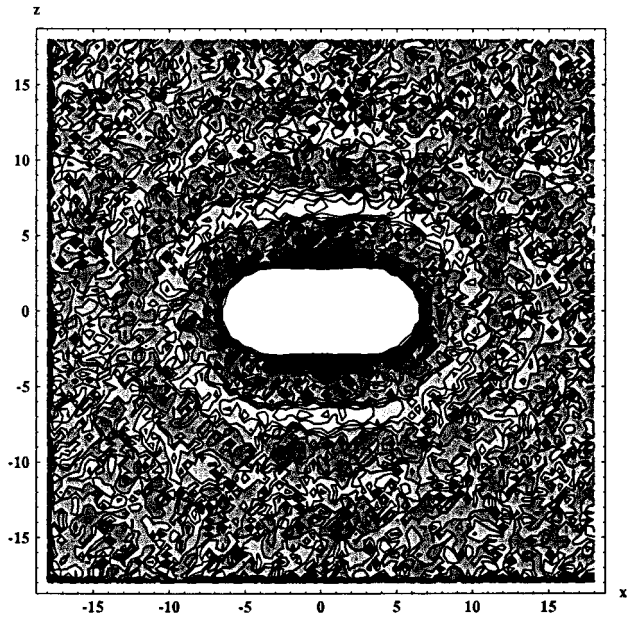

Figure 5. Distribution of cyclohexane carbons around perylene: slice in XZ plane, 300 K.

In our previous study of rotational diffusion of anthracene in cyclohexane and 2-propanol,[22] the details of solvation were different than those found here for perylene. Thus, a well defined solvation structure in the molecular plane of anthracene was found in cyclohexane, but not in 2-propanol. The presence of definite solvent residence sites implied partial stick conditions and explained the slower spinning around z in cyclohexane. Additionally, the slowing down of the tumbling around the long in-plane axis in 2-propanol was rationalized by the close contacts of the alcohol OH groups formed above and below the aromatic ring plane.[22] In contrast, we found no specific solvation features around perylene. The packing of cyclohexane around perylene is only quantitatively tighter than the packing of 2-propanol. In our model potentials anthracene and perylene have quite small atomic charges (see Methods), thus we expect specific solute−solvent interactions to be weak for both solutes. The differences in microscopic details of solvation patterns around anthracene

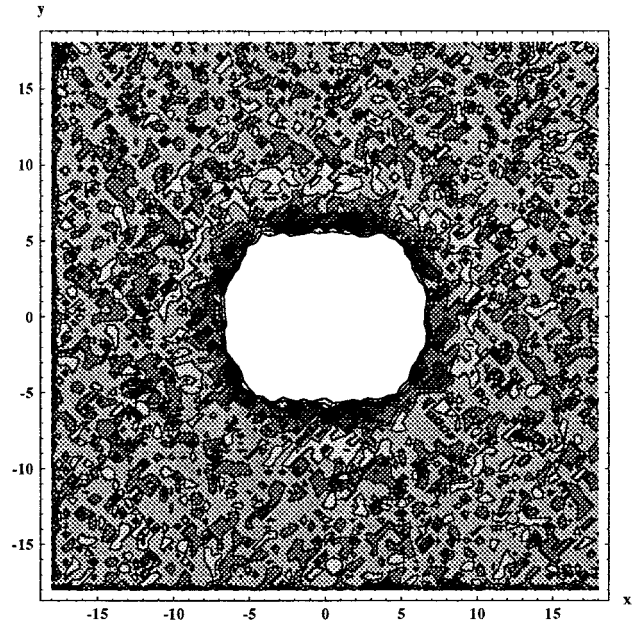

Figure 6. Distribution of 2-propanol carbons around perylene: slice in *XY* plane, 300 K.

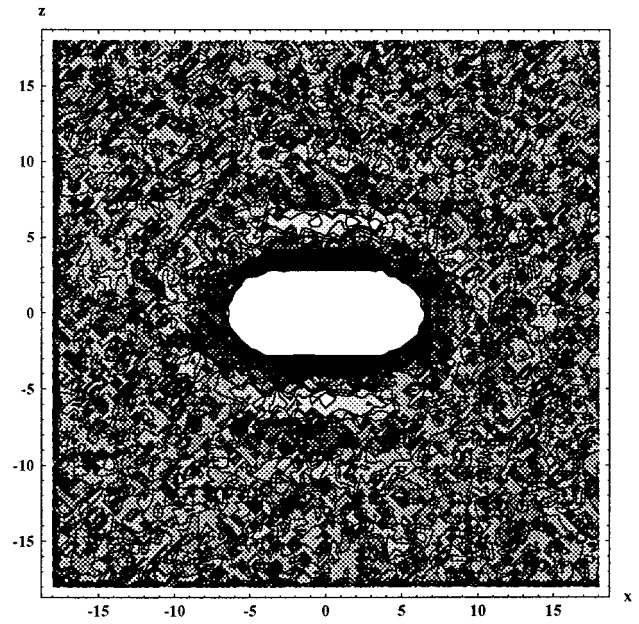

Figure 7. Distribution of 2-propanol carbons around perylene: slice in *XZ* plane, 300 K.

and perylene may thus be attributed to packing. The features found in packing of solvents around anthracene would thus appear to result from special solute/solvent size ratios, which enable eight well-defined cyclohexanes to reside in the anthracene plane and force 2-propanol OH groups to approach close to the anthracene plane in order to maintain chains of alcohol-alcohol hydrogen bonds.

Our simulation system size is large enough to accommodate between 3 and 4 solvation layers around the solute inside the primary simulation cell. Also, in Figures 4−8, the solvent distribution is close to uniform at the edges of the cells. Taken together with the good agreement of the calculated and observed rotational relaxation times (see below), it appears that the solvent cell size and simulation length are sufficient to correctly model perylene rotational dynamics in dilute solution.

Experimental Results: Pump and Probe Transitions. Perylene was excited into the $S_1(^1B_{3u})$ excited state with pump

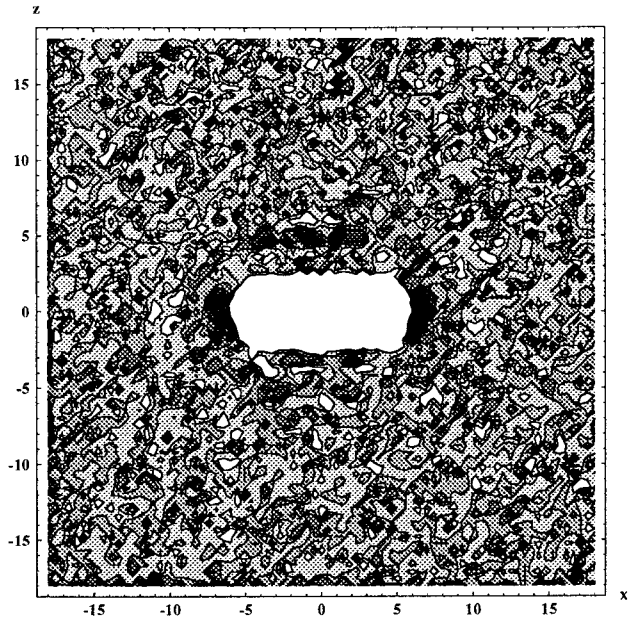

Figure 8. Distribution of 2-propanol oxygens around perylene: slice in *XZ* plane, 300 K.

pulses at 400 nm. This absorption band is characterized by a transition dipole lying along the long in-plane (*x*) axis of the molecule with constant polarization through the band (450 nm − 360 nm).[57,58] Linear dichroism signals were recorded with probe pulses at 470, 600, or 650 nm. At these wavelengths, the appearance of the isotropic transient absorption signal (calculated as $\Delta A_{\parallel} + 2\Delta A_{\perp}$) is instrument limited. The transient absorption decays slightly over the time scale scanned in these experiments (data not shown), consistent with the fluorescence lifetime of ca. 4.8 ns.[30]

The transient absorption and gain spectrum of perylene has been measured previously throughout the visible region.[59] Stimulated-emission gain dominates the transient response in the 450 to 500 nm region with negligible contribution from the ground-state bleach. A broad excited-state absorption band ($S_1 \rightarrow S_n$) was also detected, resulting in a net positive transient absorption signal, ΔA, at wavelengths greater than 530 nm (in cyclohexane). Thus, the linear dichroism experiment probes the S_1 state through stimulated emission gain and excited-state absorption at the probe wavelengths employed in the linear dichroism measurements presented here. The transition dipole for stimulated emission lies along the long in-plane axis (*x*). Excited-state absorption ($S_1 \rightarrow S_n$) in the 450−700 nm region may include contributions from transitions polarized either along *x* or *y*. Calculations predict that both $B_{3u} \rightarrow A_g$ and $B_{3u} \rightarrow B_{1g}$ transitions occur in the visible and near-infrared regions with high oscillator strengths.[60]

Experimental Results: Anisotropy Decays. Experimental anisotropy decays are shown in Figure 10. The fitting parameters are given in Table 4. Data points have been omitted for times before time zero where the anisotropy is not well defined and for times during the overlap of pump and probe pulses, where the anisotropy is convoluted with the instrument function and may contain artifacts from nonlinear optical processes that may contribute to the signal.

In the present situation, where the linear dichroism contains contributions from stimulated emission and from one or more $S_1 \rightarrow S_n$ transitions, the initial anisotropy $r(0)$ can be written

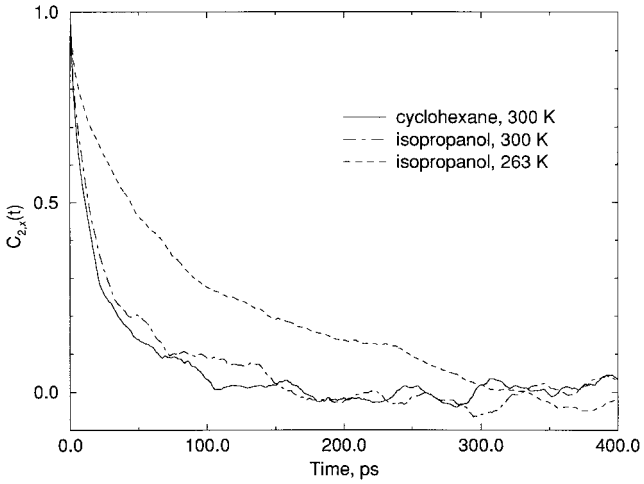

Figure 9. C_2 correlation functions of perylene in cyclohexane (at 300 K) and in 2-propanol (at 263 and 300 K) along *X*-axis of the molecule.

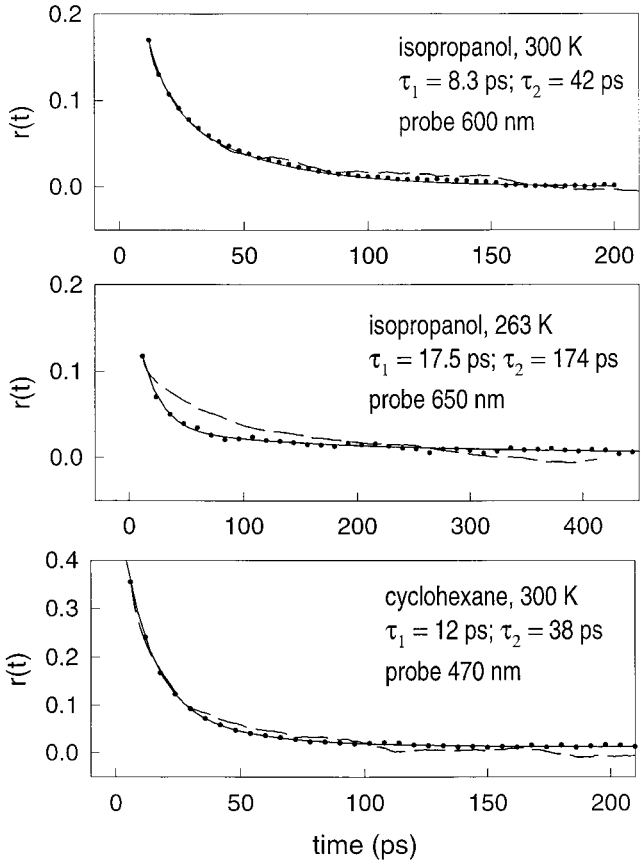

Figure 10. Anisotropy decay curves for perylene measured by time-resolved linear dichroism. The solid lines show fits of the experimental anisotropy decays (circles) to two-exponential decays. The dashed lines show the $C_{2,x}$ correlation functions from Figure 9, scaled vertically to the initial anisotropy value for each scan. Perylene was excited at 400 nm and probed at the probe wavelength indicated. Note that $t = 0$ denotes the start of the scan, not the time of maximum temporal overlap between pump and probe pulses.

$$r(0) = r_n + (r_{se} - r_n)\frac{\Delta A_{se}}{\Delta A} + \sum_{m \neq n}(r_m - r_n)\frac{\Delta A_m}{\Delta A} \quad (8)$$

where r_{se} and r_n are the initial anisotropies for the stimulated-emission and $S_1 \rightarrow S_n$ transitions, respectively, ΔA_{se} and ΔA_n are the contributions of the stimulated-emission and excited-state absorption to the transient absorption, respectively, and

$$\Delta A = \Delta A_{se} + \sum_n \Delta A_n \quad (9)$$

Note that ΔA_{se} is negative whereas the ΔA_n are positive. If all of the contributing transition dipoles are parallel, the initial anisotropy $r(0)$ will be 0.4, the value expected in the case of a single probe transition having a transition dipole parallel to the pump transition dipole. However, if as expected the excited-state absorption contains contributions from transition dipoles that are not parallel to the transition dipole for stimulated emission, the initial anisotropy may be lower than 0.4. We expect, therefore, that for probe wavelengths in the region dominated by stimulated emission, the initial anisotropy value will approach 0.4, whereas for probe wavelengths farther to the red, with stronger excited-state absorption contributions, lower initial anisotropy values may arise. This is in fact what we observe. For perylene in cyclohexane, we detect an initial anisotropy value of 0.33 for a 470 nm probe wavelength. This value is consistent with r(0) values in the range 0.31 to 0.37 that have been observed in fluorescence studies.[29,30,61,62] In contrast, for a probe wavelength of 600 nm, where excited-state absorption is stronger than stimulated-emission gain, we have measured r(0)=0.25 for perylene in cyclohexane. The decrease in r(0) probably results from contributions from an $S_1 \rightarrow S_n$ transition that is not polarized along the long axis. Such a transition has been predicted to occur in this region of the transient absorption spectrum.[60]

For perylene in 2-propanol, an initial anisotropy of 0.23 was found for a probe wavelength of 500 nm, where a net gain is observed. Initial anisotropies of 0.17 and 0.10 were measured for probe wavelengths of 600 and 650 nm, respectively, where a net absorption is observed. These values follow the pattern observed for perylene in cyclohexane, with a higher $r(0)$ measured for a probe wavelength in the stimulated emission gain region. The decreased value of $r(0)$ at 650 nm compared to 600 nm may result from an enhanced contribution from an excited-state absorption transition with transition dipole along y. However, in addition to the dependence of $r(0)$ on the probe wavelength, the value of $r(0)$ appears to be lower in 2-propanol than in cyclohexane. This may be a result of solvent-dependent shifts in the underlying transient absorption spectra contributing to the observed $r(0)$ (see eq 8). Nevertheless, as described above, the observed value of $r(0)$ is determined by overlapping electronic transitions and fast librational or structural dynamics that apply to all molecules in the same way, regardless of orientation and therefore are not expected to affect the measured rotational dynamics. It should be noted, however, that the measured anisotropy decay is not purely associated with the *x* axis. Initial anisotropy values of less than 0.4 indicate contributions from a transition polarized along y. This transition will not affect the rotational time constants but may affect the amplitudes of the two components. However, even for $r(0) = 0.17$, *x*-axis transition dipoles dominate the transition.

The experimental anisotropy decays are shown in Figure 10. These decays were fit with two-exponential decay functions. Two time constants in the anisotropy decay of perylene have been observed previously in several cases for highly viscous solvents.[25,27−32,63−65] With the availability of subpicosecond laser sources, it is now possible to measure the rotational relaxation of perylene in less viscous solvents. Although the experimental measurements probe the S_1 state of perylene rather than the S_0 state, differences in ground and excited-state rotational dynamics are expected to be negligible.[24]

The experimental results illustrate the difference in coupling of rotational motions to the solvent environment in cyclohexane

TABLE 4: Fitting Parameters for Measured and Simulated Anisotropy Decays

solvent	T (K)	probe wavelength (nm)	measured[a]					simulated	
			τ_1 (ps)	r_1	τ_2 (ps)	r_2	r(0)	τ_1 (ps)	τ_2 (ps)
cyclohexane	300	470	13.5 ± 1.5	0.26 ± 0.02	52 ± 16	0.07 ± 0.02	0.33 ± 0.04	9 ± 4	44 ± 9
cyclohexane	300	600	8.4	0.22	48.4	0.32	0.25		
2-propanol	300	600	9.8 ± 2.1	0.08 ± 0.01	51 ± 11	0.09 ± 0.02	0.17	13 ± 3	75 ± 21
2-propanol	300	500	18	0.18	136	0.06	0.23		
2-propanol	300	650	14.5	0.06	72	0.04	0.10		
2-propanol	263	650	22.2 ± 2	0.08 ± 0.02	240 ± 80	0.02 ± 0.01	0.10	25 ± 4	126 ± 30

[a] Values with errors are averages from several data sets. Errors are the standard deviation in the mean.

and 2-propanol. Simple hydrodynamic theory predicts that the quantity $\tau_i T/\eta$ (where $i = 1,2$ labels the anisotropy decay component) should be constant. A comparison shows, however, that the ratios $\tau_1 T/\eta$ and $\tau_2 T/\eta$ are smaller in 2-propanol than in cyclohexane. For example, at 300 K, the value $\tau_1 T/\eta$ is 4.5×10^3 ps·K/cP in cyclohexane compared to 1.5×10^3 ps·K/cP in 2-propanol. Similarly, the value of $\tau_2 T/\eta$ is 17×10^3 ps·K/cP in cyclohexane compared to 8.1×10^3 ps·K/cP in 2-propanol. These observations are consistent with previous reports of faster rotational relaxation in alcohols compared to other solvents such as alkanes for a given viscosity.[23] This "sub-slip" behavior has previously been attributed to a lower microscopic viscosity experienced by a solute. As discussed in the next section, molecular dynamics simulations provide additional insight into this behavior.

In a recent study, Goldie and Blanchard[25] reported the rotational diffusion dynamics of perylene in a series of n-alcohols. Anisotropy decays with two time components were observed. The ratio D_z/D_x of diffusion coefficients for spinning about the z axis relative to tumbling about the x axis was found to increase with solvent chain length, demonstrating increasingly anisotropic diffusion. This observation is consistent with our results for perylene in 2-propanol and adds further support to the picture of larger D_z/D_x ratios in alcohols relative to alkanes (see the following section). In contrast, in an earlier study of perylene in *n*-alkanes,[24] only single time components were observed in the anisotropy decays. Because the viscosity range in that work overlaps the viscosities of the solvents in our study, a comparison with their results is relevant. Jiang and Blanchard observed two regimes in the viscosity dependence of perylene rotational diffusion in *n*-alkanes. For *n*-pentane to *n*-octane, a linear viscosity dependence with $\tau T/\eta = 12 \times 10^3$ ps·K/cP was found. In contrast, for the solvents *n*-nonane to n-hexadecane, the slope was 3.8×10^3 ps·K/cP. It was noted that the break in the viscosity dependence occurs at about the point where the solvent length is approximately the length of the perylene molecule. In both regimes, however, only a single-exponential anisotropy decay was detected. In comparing our results for cyclohexane to those of Jiang and Blanchard, we note that the slope of 12×10^3 ps·K/cP observed for the shorter chain alkanes corresponds roughly to our result for the slower time constant τ_2. This is reasonable because the faster time constant, τ_1 probably would not have been detectable with the 10 ps time resolution available in that study. In contrast, for the longer chain alkanes, the reported slope of 3.8×10^3 ps·K/cP matches roughly the value of $\tau_1 T/\eta$ that we observe for the faster of the two rotational time constants, τ_1 (see Table 4). This suggests that the amplitude of the slower rotational component in longer chain alkanes may become too small to be detected.

Comparison of Simulations with Experimental Results. Table 3 describes the C_2 correlation functions derived directly and indirectly from our simulations and from hydrodynamic models. The C_2 traces, values of the two relaxation times τ_1 and τ_2, as well as weights of the two exponents are directly comparable to experimental data (see Methods). The $C_{2,x}(t)$ decays obtained from the simulations are shown in Figure 9. A comparison of experimental anisotropy decays and simulated C_2 functions is shown in Figure 10.

Direct fitting of perylene $C_{2,x}(t)$ to two-exponential decay yields relaxation times τ_1, τ_2 of 25 ± 4 and 126 ± 30 ps in 2-propanol at 263 K, 13 ± 3 and 75 ± 21 ps in 2-propanol at 300 K, and 9 ± 4 and 44 ± 9 ps in cyclohexane at 300 K. These results are in excellent agreement with the experimental measurements under the same conditions: 22 ± 2 and 240 ± 80 ps, 10 ± 2 and 51 ± 11 ps, and 13.5 ± 1.5 and 52 ± 16 ps, respectively. An alternative, indirect, approach is to calculate τ_1 and τ_2 from their defining formulas (see Methods), using the basic parameters D_x, D_y, D_z obtained from fitting the C_1 correlation functions (Table 2). This leads to predictions of τ_1, τ_2 equal to 51 ± 30 and 128 ± 80 ps in 2-propanol at 263 K, 14 ± 3 and 66 ± 30 ps in 2-propanol at 300 K, and 14 ± 3 and 35 ± 20 ps in cyclohexane at 300 K. These values agree with both the direct calculations and experimental measurements, although the statistical errors of the relaxation times are larger in the indirect approach, especially for τ_1 in the low temperature 2-propanol simulation. The excellent agreement with available experimental data indicates that our simulations provide a realistic model for rotational diffusion of perylene in organic solvents, supporting the reliability of the detailed description of rotational anisotropy and microscopic solute−solvent interactions emerging from the simulation results.

Both the experimental anisotropy (Figure 10) and the simulated C_2 correlation functions decay with two exponential components in both 2-propanol and cyclohexane, as expected for an asymmetric rotor with the transition dipole aligned along one of its principal axes (eq 4). These two components in the rotational relaxation have been previously interpreted within the simplified but appealing model of perylene reorienting roughly as an oblate rotor, with a large difference in diffusion coefficients for reorientation about the axis normal to the plane of the molecule (D_z) relative to reorientation about axes in the molecular plane ($D_x = D_y$). For an oblate rotor, the ratio of relaxation times is given by[66]

$$\frac{\tau_2}{\tau_1} = \frac{2D_z}{3D_x} + \frac{1}{3} \tag{10}$$

Thus, the large value of the D_z diffusion coefficient relative to D_x, and D_y is responsible for the large difference in the two relaxation times, τ_1 and τ_2. The simulations bear this out qualitatively, with D_z a factor of 2.4 (for cyclohexane) to 4.6 (for 2-propanol) times as large as D_x. However, the simulations also reveal that perylene is not a perfect oblate rotor. The diffusion coefficients for reorientation about x and y are different by about a factor of 2, rather than being equal as they would be for an oblate rotor. Thus, treatments that consider perylene as an oblate rotor, although qualitatively correct, are oversimplified.

The simulations provide a microscopic explanation for these experimental observations. A comparison of the rotational diffusion coefficients calculated for 2-propanol and cyclohexane at 300 K shows a roughly 2-fold increase in D_x and D_y in 2-propanol relative to cyclohexane (Table 2), consistent with the viscosity increases by a factor of about 2. However, it is D_z that is largely responsible for the different relaxation in cyclohexane and 2-propanol. Although the viscosity is 2.0 cP in 2-propanol compared to 0.9 cP in cyclohexane, D_z is actually slightly higher in 2-propanol. Thus, the faster rotational relaxation in 2-propanol for a given viscosity compared to cyclohexane can be attributed to faster spinning of the molecule about the axis normal to the plane. This result is compatible with recent observations; an analysis of the two-photon induced anisotropy decays showed that the differences in anisotropy decay following linearly and circularly polarized two-photon excitation is consistent with a larger ratio of D_z to D_x or D_y in alcohols than in alkanes.[26]

A comparison of the rotational decay times in the two solvents, cyclohexane and 2-propanol, reveals further that the ratio τ_2/τ_1 is larger in 2-propanol at 263 K than at 300 K. According to hydrodynamic theory, the rotational correlation times depend only on solute size and shape, on solvent viscosity, and on hydrodynamic boundary conditions. Thus, the temperature dependence of the τ_2/τ_1 ratio bears witness to nonhydrodynamic features in the rotational dynamics. The larger τ_2/τ_1 ratio at 263 K corresponds to more anisotropic diffusion, i.e., a larger ratio of D_z to D_x or D_y. In other words, the principal diffusion coefficients are less uniform in 2-propanol at 263 K than at 300 K, leading to faster in-plane spinning relative to out-of-plane tumbling at 263 K.

Conclusions

We have employed both time-resolved linear dichroism measurements and molecular dynamics simulations to investigate the rotational diffusion of perylene as a function of temperature and solvent type. The linear dichroism measurements yielded rotational reorientation times for the $S_0 \rightarrow S_1$ transition dipole (*x* axis in our notation). Molecular dynamics simulations were used to calculate the average rotational diffusion coefficients, diffusion coefficients and reorientation correlation functions for the individual molecular axes, as well as the average distribution of solvent molecules around perylene in solution. Both experiments and simulations yielded a biexponential anisotropy decay $C_{2x}(t)$. The calculated time constants for reorientation of the perylene *x* axis were 25 and 126 ps in 2-propanol at 263 K, 13 and 75 ps in 2-propanol at 300 K, and 9 and 44 ps in cyclohexane at 300 K, in excellent agreement with the corresponding experimental results of 22 and 240 ps, 10 and 51 ps, and 14 and 52 ps, respectively. The close agreement of calculated and observed rotational relaxation times indicates that the simulations realistically model the rotational diffusion of perylene at different temperatures and in different solvents. This strongly supports the reliability of the unexpected features of perylene reorientational dynamics emerging from the simulation results.

Analysis of the calculated rotational diffusion coefficients for the individual molecular axes of perylene uncovered several interesting features. The diffusion is highly anisotropic, with the fastest rotation around the out-of-plane axis (*z*) under all simulated conditions, as expected for an oblate-like ellipsoid. What is surprising is that this rotation proceeds at approximately the same rate for perylene in 2-propanol and cyclohexane at room temperature. On the other hand, tumbling around the in-plane axes (*x* and *y*) is slower by about a factor of 2 in 2-propanol compared to cyclohexane, in accord with hydrodynamic predictions. Because the rotational diffusion coefficient D_z is much larger than D_x or D_y, the overall result is only a small change in the average rotational diffusion coefficient D_r between 2-propanol and cyclohexane. This is a demonstration of a breakdown of the simple hydrodynamic description of rotational diffusion. A microscopic explanation for these effects is provided by analysis of the solvent structure around perylene. The first solvation shells formed in the perylene plane by cyclohexane and 2-propanol are qualitatively similar, featuring essentially structureless bands of enhanced solvent density. A closer look reveals that cyclohexane is able to approach ca. 0.5 Å closer to the solute than 2-propanol along the short in-plane axis (*y*). Thus, the similarity of the D_z coefficients of perylene in cyclohexane and 2-propanol may be attributed to specific hindrance of spinning motion due to solvent packing in the former system.

It is interesting to compare the perylene results described here with our previous study of rotational diffusion of anthracene in the same solvents.[22] In the anthracene case, the simulation results for the rotational correlation time τ_1 were also in good agreement with experimental measurements. Calculated average rotational diffusion coefficients of anthracene followed hydrodynamic predictions for a triaxial ellipsoid under slip conditions. However, an analysis of the simulation results for reorientation rates around individual molecular axes revealed a pattern of nonuniform changes with temperature and solvent. The most striking effect was the change of the fastest rotational mode from tumbling around the long in-plane axis in cyclohexane to spinning around the molecular plane normal in 2-propanol. The selective slowing down of anthracene spinning in cyclohexane is analogous to the effect seen for perylene in this study. However, the molecular mechanism of this phenomenon appears to be different for the two solutes. The solvation patterns of cyclohexane and 2-propanol around perylene are qualitatively similar and differ only in quantitative details. For anthracene, qualitative differences in solvation were found, with specific clustering of cyclohexanes in the solute plane and close contacts of 2-propanol OH groups above and below the plane. The presence of these specific features appears to be due to special solute/solvent size ratios, which no longer apply for the larger perylene molecule.

Both our current simulations of perylene and the previous study of anthracene suggest that the frictional coupling to the solvent may be different for reorientational motions about different molecular axes of the solute. For anthracene the apparent success of the SED equation in predicting the average rotational correlation time appears to disguise interesting, nonhydrodynamic effects in the rotational dynamics for individual molecular axes. For perylene, even the average diffusion coefficients are in disagreement with SED theory. Both these effects may be explained qualitatively by analyzing local solvent structure. Interestingly, the solvent distributions around anthracene and perylene were predicted to be markedly different from each other, most probably due to the different solute/solvent size ratios in these two systems.

Overall, our results show the synergy of the joint experimental/computational approach. Once the simulation results are validated by comparison with available experimental data, the detailed modeling results may be used to uncover interesting and informative details of molecular reorientations in solution that are difficult to extract from experimental data alone. Especially the calculation of reorientation rates around individual

molecular axes allows probing specific solute−solvent interactions and the microscopic effects of solvent structure. Our results for the relatively simple and rigid anthracene and perylene solutes should be a good starting point on the way to simulating diffusion of more complex systems, covering a wider range range of solute/solvent size ratios, including specific interactions and internal flexibility, such as tethered chromophoric probes or peptides.

Acknowledgment. The authors would like to thank Terra Computers Inc., for use of the TR2016 computer and the Center for Advanced Scientific Computing at the University of Kansas for use of the ORIGIN 2000 computer system. G.S.J. would like to thank Attila Szabo and Robert W. Zwanzig for helpful discussions, and Alexnder M. Berezhkovskii for critical reading of the manuscript.

References and Notes

(1) Einstein, A. *Investigations on the Theory of Brownian Movement*; Dover: New York, 1956.

(2) Hynes, J. T.; Kapral, R.; Weinberg, M. *J. Chem. Phys.* **1978**, *69*, 2725−2733.

(3) Dote, J. L.; Kivelson, D. *J. Phys. Chem.* **1983**, *87*, 3889−3893.

(4) Ben-Amotz, D.; Scott, T. W. *J. Chem. Phys.* **1978**, *87*, 3739.

(5) Eimer, W.; Pecora, R. *J. Chem. Phys.* **1991**, *94*, 2324.

(6) Cantor, C. R.; Schimmel, P. R. *Biophysical Chemistry: Techniques for the Study of Biological Structure and Function*; W. H. Freeman, New York 1980, Vol. 2

(7) Perrin, F. *J. Phys. Radium* **1934**, *5*, 497.

(8) Perrin, F. *J. Phys. Radium* **1936**, *7*, 1−11.

(9) Hu, C.-M.; Zwanzig, R. *J. Chem. Phys.* **1974**, *60*, 4354−4357.

(10) Dote, J. L.; Kivelson, D.; Schwartz, R. N. *J. Phys. Chem.* **1981**, *85*, 2169−2180.

(11) Youngren, G. K.; Acrivos, A. *J. Chem. Phys.* **1975**, *63*, 3846−3848.

(12) Sension, R. J.; Hochstrasser, R. M. *J. Chem. Phys.* **1993**, *98*, 2490.

(13) de la Torre, J. G.; Carrasco, B. *Biophys. J.* **2000**, *78*, 719−730.

(14) Liu, H.; Muller-Plathe, F.; van Gunsteren, W. F. *J. Am. Chem. Soc.* **1995**, *117*, 4363−4366.

(15) Zhang, Y.; Venable, R. M.; Pastor, R. W. *J. Phys. Chem.* **1996**, *100*, 2652−2660.

(16) Brodka, A.; Zerda, T. W. *J. Chem. Phys.* **1996**, *104*, 6313−6318.

(17) Benmore, C. J.; Loh, Y. L. *J. Phys. Chem.* **2000**, *112*, 5877−5883.

(18) Smith, P. E.; van Gunsteren, W. F., *J. Mol. Biol.* **1994**, *236*, 629−636.

(19) Brown, R.; Middelhoek, R.; Glasbeek, M. *J. Chem. Phys.* **1999**, *111*, 3616−3622.

(20) Hu, Y.; Fleming, G. R. *J. Chem. Phys.* **1991**, *94*, 3857−3866.

(21) Luzar, A.; Chandler, D. *J. Chem. Phys.* **1993**, *98*, 8160−8173.

(22) Jas, G. S.; Wang, Y.; Pauls, S. W.; Johnson, C. K.; Kuczera, K. *J. Chem. Phys.* **1997**, *107*, 8800−8812.

(23) Williams, A. M.; Jiang, Y.; Ben-Amotz, D. *Chem. Phys.* **1994**, *180*, 119−129.

(24) Jiang, Y.; Blanchard, G. J. *J. Phys. Chem.* **1994**, *98*, 6436−6440.

(25) Goldie, S. N.; Blanchard, G. J. *J. Phys. Chem. A* **1999**, *103*, 999−1006.

(26) Pauls, S. W.; Hedstrom, J. F.; Johnson, C. K. *Chem. Phys.* **1998**, *237*, 205−222.

(27) Brocklehurst, B.; Young, R. N. *J. Phys. Chem. A* **1999**, *103*, 3809−3817.

(28) Brocklehurst, B.; Young, R. N. *J. Phys. Chem.* **1995**, *99*, 40−43.

(29) Piston, D. W.; Bilash, T.; Gratton, E. *J. Phys. Chem.* **1989**, *93*, 3963−3967.

(30) Lakowicz, J. R.; Cherek, H.; Maliwal, B. P.; Gratton, E. *Biochemistry* **1985**, *24*, 376−383.

(31) Christensen, R. L.; Drake, R. C.; Phillips, D. *J. Phys. Chem.* **1986**, *90*, 5960−5967.

(32) Zinsli, P. E. *Chem. Phys.* **1977**, *20*, 299−309.

(33) Brooks, B. R.; Bruccoleri, R.; Olafson, B.; States, D.; Swaminathan, S.; Karplus, M. *J. Comput. Chem.* **1983**, *4*, 187−217.

(34) MacKerell, A. D., Jr.; Bashford, D.; Bellott, M.; Dunbrack, R. L., Jr.; Evanseck, J. D.; Field, M. J.; Fischer, S.; Gao, J.; Guo, H.; Ha, S.; Joseph-McCarthy, D.; Kuchnir, L.; Kuczera, K.; Lau, F. T. K.; Mattos, C.; Michnick, S.; Ngo, T.; Nguyen, D. T.; Prodhom, B.; Reiher, W. E., III.; Roux, B.; Schlenkrich, M.; Smith, J. C.; Stote, R.; Straub, J.; Watanabe, M.; Wiorkiewicz-Kuczera, J.; Karplus, M. *J. Phys. Chem. B* **1998**, *102*, 3386−3616.

(35) Frisch, C. M. J.; Trucks, G. W.; Head-Gordon, M.; Gill, P. M. W.; Wong, M. W.; Foresman, J. B.; Johnson, B. G.; Schlegel, H. B.; Robb, M. A.; Replogle, E. S.; Gomperts, R.; Andres, J. L.; Raghavachari, K.; Binkley, J. S.; Gonzalez, C.; Martin, R. L.; Fox, D. J.; Defrees, D. J.; Baker, J.; Stewart, J. J. P.; Pople, J. A., *GAUSSIAN92, Revison C*, Gaussian, Inc., Pittsburgh, PA **1992**.

(36) Jas, G.; Kuczera, K. *Chem. Phys.* **1997**, *214*, 229−241.

(37) Cox, S. R.; Williams, D. E. *J. Comput. Chem.* **1981**, *2*, 204.

(38) Jas, G. S.; Kuczera, K

(39) Weast, R. C., Ed. *CRC Hand Book of Chemistry and Physics, 66th ed.;* CRC Press: Cleveland, OH 1985−1986.

(40) Ryckaert, J. P.; Ciccotti, G.; Berendsen, H. J. C. *J. Comput. Phys.* **1977**, *23*, 327−341.

(41) Barth, E.; Kuczera, K.; Leimkuhler, B.; Skeel, R. D. *J. Comput. Chem.* **1995**, *16*, 1192−1209.

(42) Verlet, L. *Phys. Rev.* **1967**, *159*, 98.

(43) Feller, S. E.; Zhang, Y.; Pastor, R. W. *J. Chem. Phys.* **1995**, *103*, 4613−4621.

(44) Hoover, W. G. *Phys. Rev. A* **1985**, *31*, 1695−1697.

(45) McConnell, J. *Rotational Brownian Motion and Dielectric Theory*; Academic Press: London 1980.

(46) Zwanzig, R.; Bixon, M. *Phys. Rev. A* **1970**, *2*, 2005.

(47) Hwang, L. P.; Freed, J. H. *J. Chem. Phys.* **1975**, *63*, 118.

(48) Ehrenberg, M.; Rigler, R. *Chem. Phys. Lett.* **1972**, *14*, 539−544.

(49) Chuang, T. J.; Eisenthal, K. B. *J. Chem. Phys.* **1972**, *57*, 5094−5097.

(50) Chalikian, T.; Breslauer, K. *Biopolymers* **1996**, *39*, 619.

(51) Riddick, J. A.; Bunger, W. B.; Sakand, T. K. *Organic Solvents: Physical Properties and Methods of Purification*; John Wiley and Sons: New York 1986.

(52) Quitevis, E. L.; Horng, M. L. *J. Phys. Chem.* **1980**, *94*, 5684.

(53) Bessire, R. D.; Quitevis, E. L. *J. Phys. Chem.* **1994**, *98*, 13083.

(54) Bauer, D. R.; Alms, G. R.; Brauman, J. I.; Pecora, R. *J. Chem. Phys.* **1973**, *59*, 5321.

(55) Bauer, D. R.; Brauman, J. I.; Pecora, R. *J. Am. Chem. Soc.* **1974**, *96*, 6840.

(56) Chen, L. X. Q.; Engh, R. A.; Fleming, G. R. *J. Phys. Chem.* **1988**, *92*, 1066.

(57) Tanizaki, Y.; Yoshinaga, T.; Hiratsuka, H. *Spectrochim. Acta* **1978**, *34*, 205−210.

(58) Zimmerman, H.; Joop, N. *Z. Elektrochem.* **1961**, 138−142.

(59) Meyer, Y. H.; Plaza, P. *Chem. Phys.* **1995**, *200*, 235−243.

(60) Matsunuma, S.; Akamatsu, N.; Kamisuki, T.; Adachi, Y. *J. Chem. Phys*, **1988**, *88*, 2956−2961.

(61) Szubiakowski, J.; Balter, A.; Nowak, W.; Kowalczyk, A.; Wisniewski, K.; Wierzbowska, M. *Chem. Phys.* **1996**, *208*, 283−296.

(62) It is not well understood why an $r(0)$ of 0.4 is not observed in fluorescence experiments. Possible explanations include vibronic coupling contributions to the transition, fast librational motion (Zinsli, ref 32), and a nonplanar first excited singlet state (Szubiakowski et al., ref 61).

(63) Mantulin, W. W.; Weber, G. *J. Chem. Phys.* **1977**, *66*, 4092−4099.

(64) Barkley, M. D.; Kowalczyk, A. A.; Brand, L. *J. Chem. Phys.* **1981**, *75*, 3581−3593.

(65) Kalman, B.; Clarke, N.; Johansson, L. B. *J. Phys. Chem.* **1989**, *93*, 4608−4615.

(66) Tao, T. *Biopolymers* **1969**, *8*, 609−632.